IEEE Photonics Journal
An IEEE Photonics Society Publication

Open Access

Multiwavelength Hybrid Fiber Raman/ Parametric Linear Oscillator

Volume 7, Number 4, August 2015

L. T. Lim
K. S. Yeo
M. H. Abu Bakar
N. Tamchek
F. R. Mahamd Adikan
M. A. Mahdi

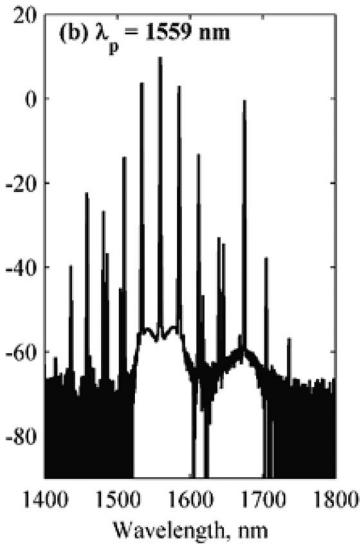

DOI: 10.1109/JPHOT.2015.2438443
1943-0655

IEEE photonics SOCIETY

IEEE

Multiwavelength Hybrid Fiber Raman/ Parametric Linear Oscillator

L. T. Lim,[1] K. S. Yeo,[2] M. H. Abu Bakar,[1] N. Tamchek,[1] F. R. Mahamd Adikan,[2] and M. A. Mahdi[1]

[1]Research Centre of Excellence for Wireless and Photonic Network, Faculty of Engineering, Universiti Putra Malaysia, 43400 Serdang, Malaysia
[2]Department of Electrical Engineering, Faculty of Engineering, University of Malaya, 50603 Kuala Lumpur, Malaysia

DOI: 10.1109/JPHOT.2015.2438443

Manuscript received March 18, 2015; revised May 8, 2015; accepted May 11, 2015. Date of publication June 1, 2015; date of current version June 24, 2015. This work was supported in part by the Ministry of Education, High Impact Research under Grant A000007-50001 and in part by the National Science Fellowship, Ministry of Science, Technology, and Innovation. Corresponding author: M. A. Mahdi (e-mail: mam@upm.edu.my).

Abstract: We demonstrate a linear cavity wideband multiwavelength fiber-based optical parametric oscillator consisting of four fiber Bragg gratings (FBGs). The FBGs center wavelengths are chosen such that they are 3.2 THz (26 nm) and 14.3 THz (115 nm) away from the parametric pump wavelength, with each located in the dominant region of parametric and Raman gain, respectively. Investigation shows that interplay between the lasing processes from the parametric and Raman gain region can be carefully adjusted to produce multiwavelength lasers spanning from 1436 to 1704 nm, with optical signal-to-noise ratio ranging from 14.3 to 54.0 dB.

Index Terms: Parametric oscillators and amplifiers, nonlinear optics, stimulated Raman scattering, fiber lasers.

1. Introduction

Over the past few decades, extensive research has been directed to develop multiwavelength fiber laser (MW-FL) due to their potential applications in wavelength division multiplexing (WDM) communication systems [1], optical sensor systems [2], microwave photonics [3], and spectroscopy [4]. Common MW-FLs rely on either materials or nonlinear scatterings, or the combination of them. For example, in [5], a 40 nm flat broadband Brillouin-Raman fiber laser is generated in the vicinity of 1557 nm to 1597 nm. A self-seeded four-wave mixing (FWM) multiwavelength laser generation based on erbium-doped fiber spanning from 1550 nm to 1590 nm has been reported in [6]. Innovative lasing band-switching/tuning designs have been proposed for wider lasing bandwidth coverage, such as the variable lasing state erbium-doped fiber laser employing a series of mismatched long period fiber grating (FBG) from 1544 nm to 1568 nm [7], a tunable spacing multiwavelength Raman fiber laser based on superimposed chirped FBG (1520 nm to 1570 nm) [8] and a C/L-band switchable multiwavelength (MW) semiconductor optical amplifier based on dual loop mirror configuration [9]. These MW-FLs are very useful in many applications; however, their operating region is confined to the C- and L-band telecommunication window.

In the competition to obtain broad lasing bandwidth, nonlinear fiber optical parametric amplification appears to be a promising candidate because of its high gain over large bandwidth

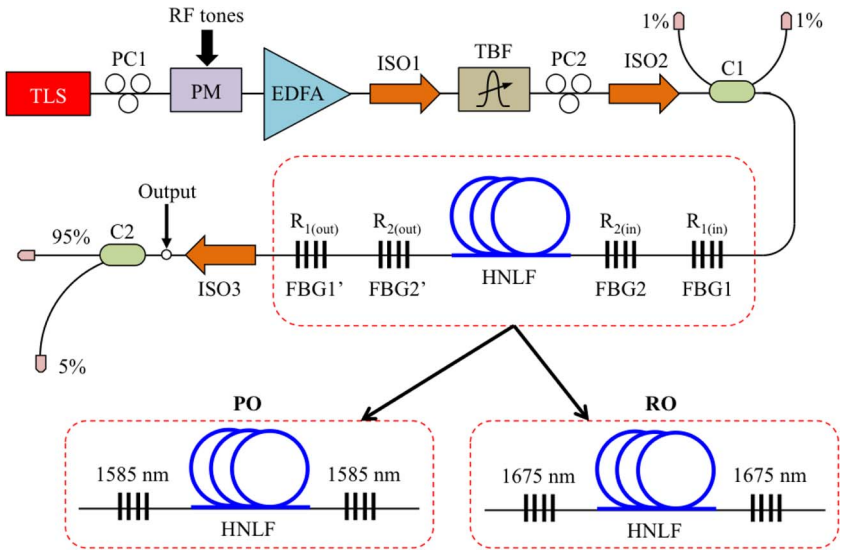

Fig. 1. Proposed setup of MW-FOPO in linear cavity configuration; the arrangement of 1585 nm and 1675 nm FBG pairs (in dashed boxes) are called PO and RO, respectively.

(> 100 nm) [10]. This characteristic has provoked interest in wideband multiple wavelengths generation based on fiber optical parametric oscillators (FOPOs). The first single-pumped MW-FOPO demonstrated by Sun *et al.* has successfully generated 0.08 nm spacing laser lines from 1510 nm to 1615 nm (total of 105 nm), using Mach–Zehnder interferometer (MZI) as the comb filter [11]. The same authors also demonstrated a 24-channel wavelength spacing tunable MW-FOPO by incorporating variable optical delay line into an MZI [12], and a 22-channel MW-FOPO with fixed wavelength spacing of 0.8 nm using Sagnac loop filter [13], both in the range of 1541 nm to 1558 nm. A transmission grating filter cascaded with programmable filter in a FOPO system is proven to be able to generate 129-channel with 25 GHz spacing, covering from 1527.58 to 1553.18 nm (25.6 nm) [14]. A superimposed chirped FBG in FOPO system has also proven to work just fine, generating 7 lasing lines of 1 nm spacing in 1550 nm region [15]. All the above FOPO experiments are limited to ring-cavity oscillators, and confined to only C- and L-band regions.

In this paper, we propose a linear-cavity MW-FOPO by using two pairs of specially fabricated FBGs with center wavelengths at 1585 nm and 1675 nm. By selecting these FBGs wavelengths, our MW-FOPO makes use of two nonlinear processes to generate lasers; parametric and stimulated Raman scattering (SRS). By deliberately manipulating the gain competition between these two processes, we obtain 14 lasing lines across 268 nm, covering from 1436 to 1704 nm with 450 mW of pump power, and laser tunability of up to 4 nm.

2. Experimental Setup and Theory

Fig. 1 shows a schematic diagram of the proposed continuous wave linear-cavity MW-FOPO. A tunable laser source (TLS) is used as the parametric pump in this setup. Along the pump path, polarization controllers PC1 and PC2 are inserted to adjust the state of polarization of the pump light. A phase modulator driven by four sinusoidal tones (100, 300, 900, and 2700 MHz) is used to broaden the linewidth of the pump light to mitigate the nonlinear effect of stimulated Brillouin scattering (SBS). An erbium-doped fiber amplifier (EDFA) is used to amplify the pump light up to a maximum of 1 W optical power. A tunable bandpass filter (TBF) with 0.8 nm bandwidth and insertion loss of 1.5 dB is inserted after the EDFA to remove excessive amplified spontaneous emission (ASE) around the pump. Two isolators (ISO1 and ISO2) are also included in the pump path to prevent any possible back reflection light from the cavity to the EDFA. A 99/1 coupler is

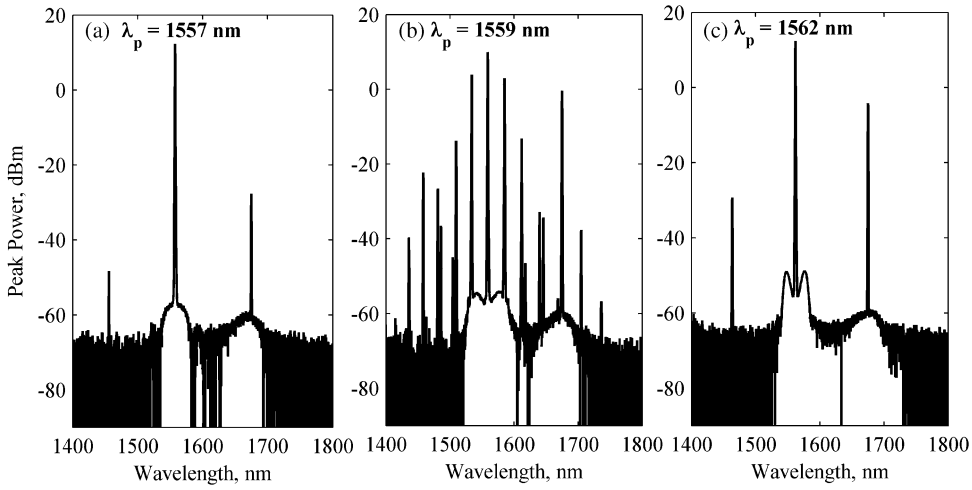

Fig. 2. Output spectra shows the impact of pump wavelength at (a) 1557 nm, (b) 1559 nm, and (c) 1562 nm.

used to couple the parametric pump into the cavity, as well as functions to monitor the pump and SBS backscattered power.

The linear cavity consists of a spool of 500 m long OFS-manufactured highly nonlinear fiber (HNLF) that is sandwiched between two pairs of FBGs. The choice of fiber length was limited to the sole available spool at our disposal. The center wavelengths chosen for the FBGs are 1585 nm (parametric dominant region) and 1675 nm (SRS dominant region). The 1585 nm FBG pair is denoted as FBG1 and FBG1′ and is dedicated for parametric oscillation (PO), whereas another FBG pair of 1675 nm is denoted as FBG2 and FBG2′ and is dedicated for Raman oscillation (RO). The reflectivity of FBG1 & FBG2 are fixed to 99% ($R_{1(in)} = 99.44\%$ and $R_{2(in)} = 99.99\%$). On the other hand, the system will be tested under four different scenarios with varying FBG1′ and FBG2′ reflectivity values in the order of 20%, 33%, 83%, and 92%. Before the output point, another isolator (ISO3) is utilized to avoid any back-reflection signals from propagating into the cavity that disrupt the lasing stability. The output spectrum of the oscillator is tapped out via the 5% port of a 95/5 coupler and connected directly to an optical spectrum analyzer (OSA). All the measurements can be back calculated to the output point as illustrated in Fig. 1.

The HNLF parameters are listed as follows: nonlinearity coefficient $\gamma = 11.5$ $W^{-1}km^{-1}$, Raman gain coefficient of 3.49 $W^{-1}km^{-1}$, zero dispersion wavelength (ZDW) $\lambda_0 = 1557.6$ nm, dispersion slope of 0.016 ps/nm^2/km, $\beta_2 = -2.888 \times 10^{-29}$ s^2/m, $\beta_3 = 2.665 \times 10^{-41}$ s^3/m, $\beta_4 = 1.321 \times 10^{-55}$ s^4/m, attenuation coefficient, $\alpha = 0.82$ dB/km, and effective area $A_{\text{eff}} = 11$ μm^2.

3. Results and Discussions

In consideration of the cavity design, the pump wavelength's location with respect to the ZDW of the fiber is crucial because the parametric gain profile is greatly determined by the choice of pump wavelength and by the dispersion properties of the fiber. In order to ensure simultaneous oscillation in parametric and Raman regime, the reflectivity for FBG1′ and FBG2′ is set at $R_{1(out)} = 92.54\%$ and $R_{2(out)} = 20.02\%$ respectively. Then, the pump wavelength is tuned around the ZDW as depicted in Fig. 2. Based on the output spectra in Fig. 2, the pump wavelength slightly above the fiber ZDW (anomalous dispersion region) at 1559 nm can satisfy the phase-matching condition since the number of laser lines is maximized from both PO and RO at a pump power of 450 mW. However, the generation of a converted idler at 1458 nm through FWM from 1675 nm lasing signal shows that the RO is likely to dominate at pump wavelength of 1552 nm and 1562 nm, due to the large wave vector mismatch that causes the parametric process to become least significant. This investigation concludes that the parametric interaction

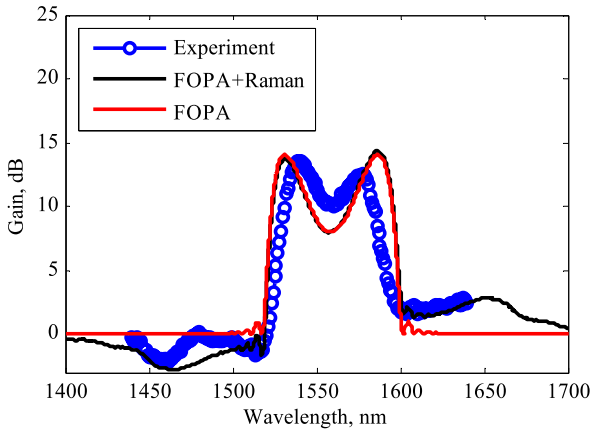

Fig. 3. Spectra comparison between theoretical and experimental phase-matched parametric gain under the influence of SRS.

is strongest when its parametric process is phase-matched [16]. By placing the pump wavelength near the fiber ZDW, the effect of group velocity can be reduced and as a result, the parametric pump wavelength is fixed at 1559 nm throughout the experiment.

A fiber optical parametric amplifier (FOPA) relies on third-order nonlinear susceptibility of the glass fiber to perform signal parametric amplification. According to theoretical studies by Shen and Bloembergen, the parametric amplification is not only dependent on parametric four-wave mixing interactions, but is also strongly associated with SRS in the third order nonlinear optical materials [17]. To make our explanation easier, this combined influence of SRS and FWM is described by a generalized nonlinear Schrodinger equation as follows [18]:

$$\frac{\partial A(z,t)}{\partial z} = -i\frac{\beta_2}{2}\frac{\partial^2 A(z,t)}{\partial t^2} + \frac{\beta_3}{6}\frac{\partial^3 A(z,t)}{\partial t^3} + i\frac{\beta_4}{24}\frac{\partial^4 A(z,t)}{\partial t^4} + i\gamma\left[(1-f)|A(z,t)|^2 + f\int_{-\infty}^{t}\chi_R^{(3)}(t-t')|A(z,t'|^2 dt'\right]A(z,t) \quad (1)$$

where $A(z,t)$ is electric field envelope, γ is the fiber nonlinear coefficient, $\chi_R^{(3)}$ is the Raman response function of silica, and f measures fractional contribution of Raman susceptibility to the Kerr nonlinearity (for fused silica $f = 0.18$). The first three terms of (1) states the dependency of parametric process on fiber dispersion while the forth term contains the complex Raman susceptibility $\chi_R^{(3)}$ to define the SRS effect in parametric amplification. A measured real and imaginary parts of the complex Raman susceptibility of fused silica is provided from previous works, where its real part is associated to parametric gain while the imaginary part of $\chi_R^{(3)}$ can be obtained from direct measurement of the Raman gain versus pump-signal frequency shift [18], [19].

In order to examine these combined effect of Raman scattering and parametric amplification processes experimentally, all FBGs were removed to form a FOPA. Based on the experimental findings, measured gain spectrum that spans from 1400 nm to 1700 nm is shown in Fig. 3 and the comparison is made by including theoretical gain spectra ($f = 0.07$ and $\lambda_p = 1559$ nm) at 0.4 W pump power, using the theoretical model in [20]. The theoretical gain curve of pure FOPA gain without Raman contribution (refer to "FOPA only") is symmetric on both sides by setting $\rho = 0$. The central gain region over the bandwidth from 1543 nm to 1587 nm represents the parametric gain with 15 dB peak gain. Around this gain region, the SRS effect is less pronounced because the parametric amplification plays the dominant role near parametric pump. The simulated gain with black solid curve shows the mixed Raman-parametric gain, which are asymmetrical with a gain peak (at approximately 100 nm away from the pump) around 1650 nm

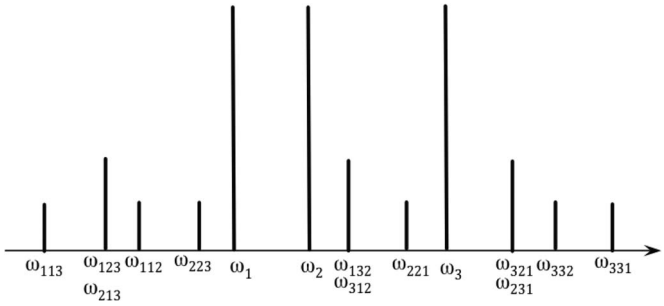

Fig. 4. Assignment of frequency components in degenerated FWM case when three input frequencies are present in the fiber.

wavelength region is detected. It is believed that the gain developed at the long wavelength region is influenced by SRS. Our experimental gain covers only from 1440 nm to 1640 nm due to the limited wavelength range of TLS used as the parametric pump, yet the influence of SRS on the phase-matched parametric gain is still observable.

The study of this Raman-parametric gain mechanism is useful to define the underlying processes of PO and RO later. Referring to the Raman-parametric gain profile in Fig. 3, the FBG wavelength is chosen at 1585 nm and 1675 nm so that one lasing signal can lase at the peak of parametric gain (near to parametric pump) while another signal can oscillate in the Raman-dominant wavelength region around 1650 nm. Lasing occurs when the net gain inside the cavity is higher than the total loss coefficient of the fiber. The total cavity loss of the linear cavity FOPO can be estimated from the sum of twice that of the accumulative fiber loss during round-trip light propagation (0.82 dB/km * 0.5 km * 2) and the finite FBG reflectivity losses that are defined according to its reflectivity values.

In our initial work, the operation of the PO and RO in the cavity is tested under four different reflectivity values for FBG1′ and FBG2′ in order to monitor the oscillation strength in each of the oscillator. The oscillation can be described in three conditions: (i) $R_{1(out)} > R_{2(out)}$, (ii) $R_{1(out)} \approx R_{2(out)}$, and (iii) $R_{1(out)} < R_{2(out)}$. In case (i), we found that PO and RO can oscillate simultaneously but at different threshold powers. For example, when $R_{1(out)} = 92.54\%$ and $R_{2(out)}$ is 20.02%, we observed that the PO started to oscillate at 300 mW pump power while RO began to oscillate at 450 mW. This combined oscillation resulted in MW laser through the process of FWM, and the number of laser lines can be predicted by using the formula $M = (N^3 - N^2)/2$, where N is the number of initial number of signal [21]. In our case, the value of N is defined by the three incident waves frequencies, which includes the pump and two lasing signals provided by the FBGs, thus resulting in nine new frequency components generated through all possible degenerate FWM process. This degenerate FWM process implies the nonlinear mixing of three distinct waves at different frequencies in an optical fiber. The process starts when the pump frequency at ω_1 propagates with a signal frequency at ω_2 (i.e., 1585 nm signal laser) in the optical fiber, where the waves interact to beat continuously with each other, leading to an intensity modulated beat note at frequency $\omega_2 - \omega_1$, which modulates the intensity-dependent refractive index of the fiber via Kerr effect [22]. When a third wave at frequency ω_3 (i.e., 1675 nm signal laser) is added, it will be phase-modulated with beat note frequency $\omega_2 - \omega_1$ due to the modulated refractive index and consequently develops sideband frequencies at $\omega_3 \pm (\omega_2 - \omega_1)$. The signal wave at ω_3 will also beat with the pump wave at ω_1, and phase-modulated ω_2 to introduce the sideband at $\omega_2 \pm (\omega_3 - \omega_1)$. The amplitude of the sidebands will be proportional to the amplitude of the signal at ω_3 and it should be noted that some FWM-product will overlap with each other [22]. Here, Fig. 4 is attached to describe the origin of multiple laser lines through degenerate FWM process in a system with three incident waves [22], [23].

On the other hand, for condition (ii) and (iii), the RO is more dominant and no oscillation could be observed from PO. It implies that when the PO and RO have equivalent reflectivity strength,

TABLE 1

Outcome of the variation in output reflectivity $R_{1(out)}$ and $R_{2(out)}$ fixed at, respectively, 20%, 33%, 83%, and 92% to the linear cavity oscillator

Reflectivity, Bandwidth		Lasing wavelength (1675 nm), $R_{2(out)}$			
		20.02% 0.70 nm	33.47% 0.62 nm	83.67% 0.76 nm	91.39% 1.14 nm
Lasing wavelength (1585 nm), $R_{1(out)}$	20.20% 0.044 nm	√	√	√	√
	33.93% 0.050 nm	√	√	√	√
	82.94% 0.048 nm	√√	√√	√	√
	92.54% 0.058 nm	√√	√√	√	√

√ : RO √√ : PO + RO

the pump is more favorable to SRS due to the long HNLF length used in the setup, even though the parametric nonlinear coefficient is larger than the Raman gain coefficient. Despite its lower gain, the SRS effect can be dominant in longer fiber lengths under certain phase-matched condition and on overlap integrals, producing about 2/3 the gain of the parametric process [16]. We have also observed that the oscillating Raman laser at 1675 nm is associated with an idler at 1458 nm, which is located symmetrically around the pump in all the cases. In short, the RO exists in all cases while the PO only exists in case (i). The oscillation summary for PO and RO is presented in Table 1. In the table, double tick indicates the operation of both PO and RO while single tick indicates the RO operation only. Here, we would like to mention that we have encountered a situation for which a slight instability occurs in case (i): if the output reflectivity of PO and RO is set at the ratio of $R_{1(out)} : R_{2(out)} = 33 : 20$, the power of MW-FL originating from PO is unstable when RO is oscillating. In this special case, we marked a single tick in Table 1, as we believe that RO is strongly depleting the energy from PO. For easy reference, Table 1 is also included with the FBGs bandwidth at their different reflectivities.

The output reflectivities of 20%, 33%, 83%, and 92% are particularly used to cover the wide range of reflectivity which allow us to observe the impact of different reflectivities on the laser performance. For the case of (ii) $R_{1(out)} \approx R_{2(out)}$ and (iii) $R_{1(out)} < R_{2(out)}$, reflectivity greater than 20% will not give any significant impact on the number of lasing lines because no matter which reflectivity values are applied, the RO will always be dominant. However, reflectivity lower than 20% could be a better choice to apply in case (i) $R_{1(out)} > R_{2(out)}$ for FBG2′ $(R_{2(out)})$, as the mitigation of SRS effect could possibly result in a stable or well-balanced oscillation between PO and RO.

It is interesting to study the operation of PO and RO individually. In this case, both oscillators are characterized separately at 450 mW pump power, with the reflectivity of FBG1′, $R_{1(out)} = 92.54\%$ and FBG2′ for $R_{2(out)} = 20.02\%$. Their output spectra are shown in Fig. 5(a), demonstrating that when the oscillator is operated in single PO mode, the lasing signal at 1585 nm (where pump-signal separation is 26 nm) induces strong FWM interaction as evidenced by generation of multiple idler lines. When the setup operates in RO mode, a strong Raman laser at 1675 nm (where pump-signal separation is 116 nm) with −7.3 dBm peak power produces an idler at 1458 nm with 20 dB optical signal-to-noise-ratio (OSNR). This has shown the extension of the FOPO oscillation bandwidth beyond the conventional parametric gain bandwidth with the assistance of SRS. Therefore, we combined these oscillators to achieve wideband MW lasers in linear cavity.

As a conclusion from our findings, the setting of output reflectivity at $R_{1(out)} = 92.54\%$ and $R_{2(out)} = 20.02\%$ provided the most stable oscillations and its output spectrum is shown in

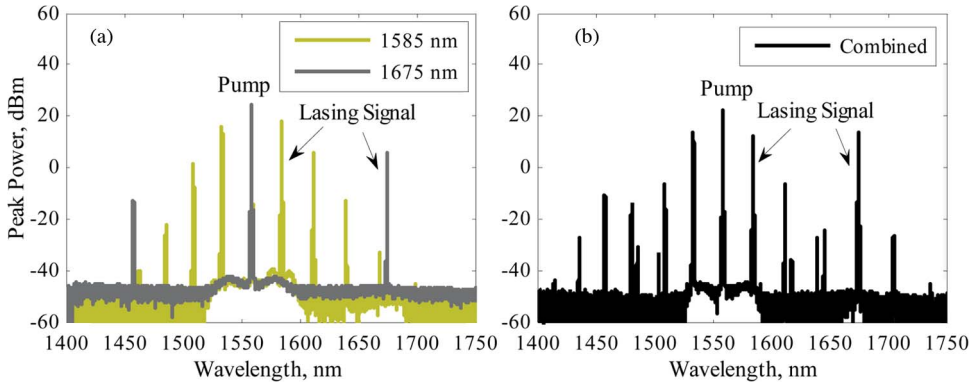

Fig. 5. Measured output spectra (a) when PO and RO are oscillated independently and (b) combined oscillation at pump power of 450 mW. The output feedback reflectivity of PO and RO is 92.54% and 20.02%, respectively.

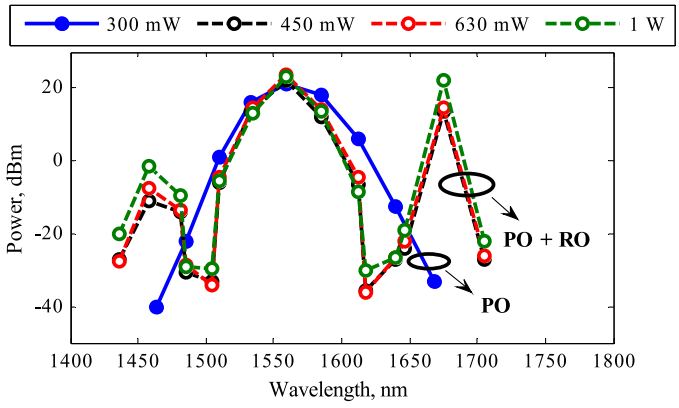

Fig. 6. Evolution of the oscillators as the pump power increases from 300 mW to 1 W.

Fig. 5(b), with MW lasers spanning from 1436 nm to 1704 nm, at which the bandwidth is widened to 268 nm, as compared to 232 nm for the case of RO. This emphasizes how oscillation strength based on the FBG reflectivity is integral in determining the mode of operation in this linear cavity MW FOPO. Furthermore, the outcome of this system has been verified to fulfill the description of a degenerate FWM process with three input frequencies, as illustrated in Fig. 4. The generated MW lasers at 1436.1 nm, 1458.2 nm, 1480.8 nm, 1485.8 nm, 1504.3 nm, 1509.4 nm, 1533.8 nm, 1611.8 nm, 1617.8 nm, 1639.7 nm, 1645.82 nm, and 1704.8 nm in this work are known as the sideband frequencies, which are developed simultaneously from mixing interaction between the pump at 1559 nm and lasing signals (1585 nm and 1675 nm). Whereas, the laser at 1415 nm and 1736 nm are ignored since they have very low output power. The number of sidebands is dependent on the amount of injected pump power and as characterized experimentally from this system, we obtained more lasers in broader wavelength range at 450 mW pump power. Based on the spectral output from OSA, the laser linewidth is measured between 0.11 nm and 0.32 nm.

Subsequent results are mainly based on the settings where $R_{1(out)} = 92.54\%$ and $R_{2(out)} = 20.02\%$ in order to guarantee a stable and balanced oscillation for further analysis. The effect of pump power increment until a maximum of 1 W to the combined oscillators is discussed first. A graph of the peak power versus laser wavelength with increasing pump power is included for discussion as depicted in Fig. 6. The minimum pump power required for PO oscillation is 300 mW. At this point, 1585 nm lasing signal is the first to be initiated together with a number of idler lines from 1462.9 nm to 1668.6 nm (bandwidth: 205.7 nm). Subsequently, combined RO

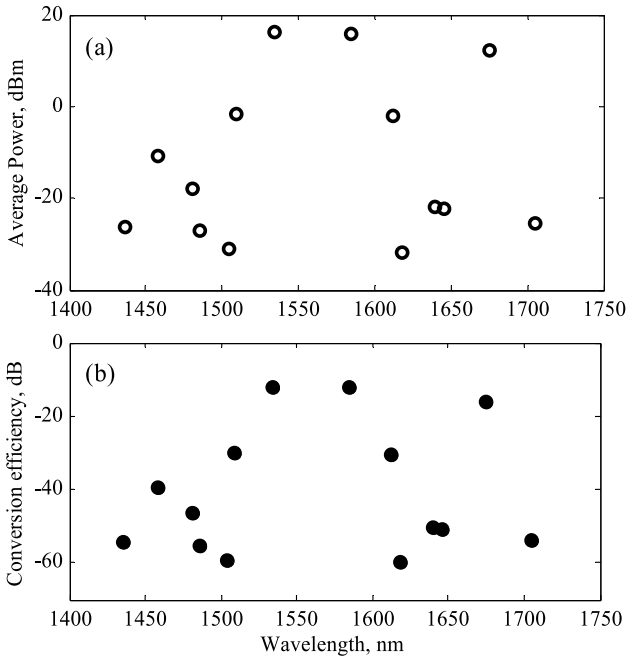

Fig. 7. (a) Graph of average power and (b) calculated conversion efficiency for lasers from 1436 nm to 1704 nm. The pump power is 630 mW and output reflectivity $R_{1(out)} = 92.54\%$ and $R_{2(out)}$ is 20.02%.

and PO lasing is initiated when the pump power is increased to 450 mW. From Fig. 3, the lasers around 1450 nm and in the vicinity of Raman laser at 1675 nm, exhibit a proportional peak power increment in accordance to the pump power. This indicates that the parametric lasers are strongly depleted and most of its energy is transferred to enhance RO operation.

Figs. 7(a) and (b) show the combined laser output in terms of average power and their conversion efficiency (ratio of the generated idler power to the pump power entering the FOPO) when the MW-FOPO is pumped at 630 mW. The FBG-formed laser at 1585 nm and its generated first-order idler at 1533.8 nm show comparable average power of about 16 dBm with -12 dB conversion efficiency, while the 1675 nm lasing signal and its associated idler at 1458 nm exhibit an average power of 12.2 dBm and -10.9 dBm, resulting in calculated conversion efficiencies of -16 dB and -39 dB, respectively. The low conversion efficiency of the Raman idler is expected due to inefficient wavelength conversion farther (217 nm) from its lasing signal. Owing to the strong parametric process near the pump region at 1559 nm, there are also multiple sidebands generated at 1509.4 nm and 1611.9 nm with average power of around -2 dBm and conversion efficiency of -30 dB. For the rest of the lasers, a minimum power of -31.7 dBm is attained with conversion efficiencies between -40 to -60 dB.

In this study, the stability evaluation of the wideband MW fiber laser when $R_{1(out)} = 92.54\%$ and $R_{2(out)} = 20.02\%$ is also performed. Referring to Fig. 8(a), multiple spectra are scanned repeatedly for a time period of 30 minutes to measure their peak power fluctuation. In our context, the peak power fluctuation is defined as the power difference between the highest and lowest peak power of a laser within the scan time of 30 minutes. Note that this result serves only as a general overview of the laser's stability, as the nature of the OSA's scanning operation makes it incapable of accurately capturing the dynamic power variation of the MW output. The graph in Fig. 8(b) is plotted to summarize the overall MW laser peak power variation obtained from Fig. 8(a). The graph demonstrates that both 1533.8 nm and 1585 nm lasers exhibit less than 1 dB peak power fluctuation but the 1675 nm laser varies within 1.7 dB. In addition to this, the MW lasers at 1436 nm, 1480.9 nm, 1485.7 nm, 1504.3 nm, 1509.4 nm, 1617.7 nm, 1645.8 nm, and 1704.9 nm are found to have lower peak power and their measured peak power variation ranges between 1 dB to 2 dB. The peak power for the remaining lasers at 1458.1 nm,

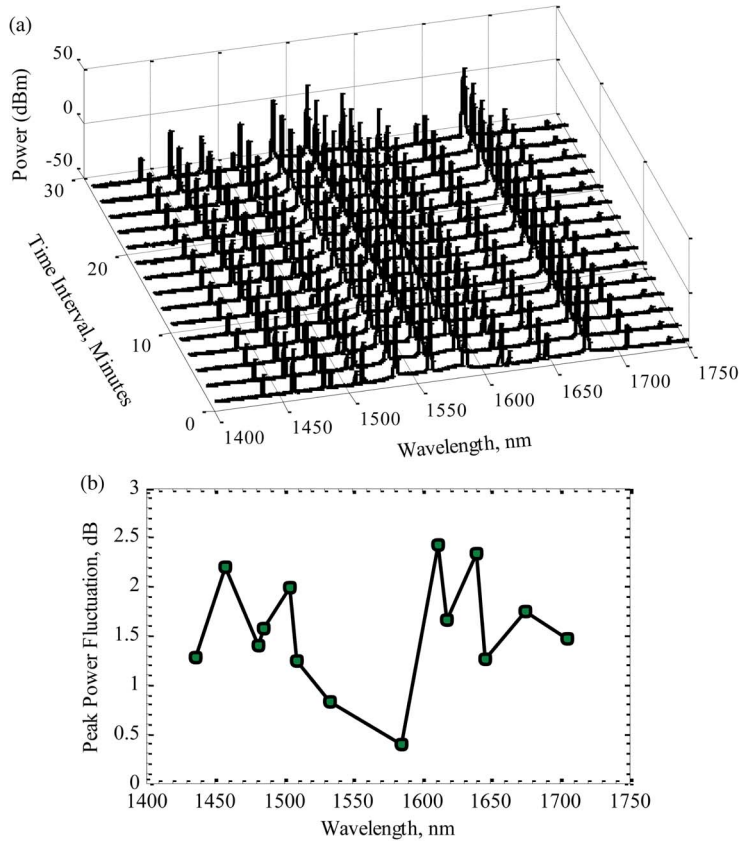

Fig. 8. Output spectra of MW lasing at pump wavelength, $\lambda_p = 1559$ nm scanned repeatedly for a time period of 30 min and (b) summary of peak power fluctuation for every peak wavelength from 1436 nm to 1704 nm during the scanning.

1611.9 nm, and 1639.8 nm, however, fluctuates by more than 2 dB, with maximum fluctuation of up to 2.4 dB observed.

Such large fluctuation was originated primarily by the unequal pump-signal wavelength separation in the system as some of the generated lasers from PO and RO, for example the lasers at 1480.8 nm, 1617.8 nm, and 1645.8 nm are looked to interfere closely with 1458.1 nm, 1611.9 nm, and 1639.8 nm lasers respectively. They withdraw energy from their adjacent lasers inconsistently and this condition has led these lasers at 1458.1 nm, 1611.9 nm, and 1639.8 nm to suffer from high power variation during the scanning time. FWM is a process that is sensitive to system parameters [21]. It is not only dependent on fiber length but is also influenced by pump-signal separation and fiber dispersion [21]. One possible way to mitigate this effect is by applying equal pump-signal separation [21] but nevertheless this method is inappropriate to be applied in our application since we wish to make use of the parametric and SRS amplification by allocating one of the signal frequencies near to the parametric pump while another signal at 100 nm (Raman-dominant region) away from the parametric pump. To resolve the unequal pump-signal separation, each signal distance from the pump should be adjusted carefully so that the output lasers from PO and RO will not interfere with each another. The problem of interference to other channels through FWM process is undesirable as it will cause signal degradation by cross-talk or excess attenuation in multichannel systems [21]. Another drawback encountered in this structure is the unequal peak power of MW lines. It is quite impossible to obtain a uniform output power because the MW lines are generated through FWM process in which the peak power of new frequency components (MW lasers) would reduce progressively as they deviate farther from the parametric pump.

4. Conclusion

A wideband MW FOPO based on cascaded FBGs in a linear cavity is experimentally demonstrated. By having one FBG pair with center wavelength in parametric dominant region and another FBG pair in Raman dominant region, the bandwidth, as well as the number of laser lines, are extended from the combined operation, compared to the operation in single oscillation mode. We have successfully demonstrated that by properly balancing the parametric and Raman gain competition in the cavity via FBG output feedback, multiple laser lines within 268 nm band from 1436 to 1704 nm are obtained, with OSNR ranging from 14.3 dB to 54 dB.

References

[1] A. E. H. Oehler, S. C. Zeller, K. J. Weingarten, and U. Keller, "Broad multiwavelength source with 50 GHz channel spacing for wavelength division multiplexing applications in the telecom C band," *Opt. Lett.*, vol. 33, no. 18, pp. 2158–2160, Sep. 2008.

[2] Y. Han, T. V. A. Tran, S. Kim, and S. B. Lee, "Multiwavelength Raman-fiber-laser-based long-distance remote sensor for simultaneous measurement of strain and temperature," *Opt. Lett.*, vol. 30, no. 11, pp. 1282–1284, Jun. 2005.

[3] Y. Yao, X. Chen, Y. Dai, and S. Xie, "Dual-wavelength erbium-doped fiber laser with a simple linear cavity and its application in microwave generation," *IEEE Photon. Technol. Lett.*, vol. 18, no. 1, pp. 2005–2007, Jan. 2006.

[4] Y. Oki, S. Miyamoto, M. Maeda, and N. J. Vasa, "Multiwavelength distributed-feedback dye laser array and its application to spectroscopy," *Opt. Lett.*, vol. 27, no. 14, pp. 1220–1222, Jul. 2002.

[5] Z. Wang *et al.*, "Broadband flat-amplitude multiwavelength Brillouin–Raman fiber laser with spectral reshaping by Rayleigh scattering," *Opt. Exp.*, vol. 21, no. 24, pp. 231–235, Dec. 2013.

[6] N. A. Cholan, M. H. Al-Mansoori, A. S. M. Noor, A. Ismail, and M. A. Mahdi, "Multi-wavelength generation by self-seeded four-wave mixing," *Opt. Exp.*, vol. 21, no. 5, pp. 6131–6138, Mar. 2013.

[7] X. Liu, L. Zhan, S. Luo, Y. Wang, and Q. Shen, "Individually switchable and widely tunable multiwavelength erbium-doped fiber laser based on cascaded mismatching long-period fiber gratings," *J. Lightw. Technol.*, vol. 29, no. 21, pp. 3319–3326, Nov. 2011.

[8] X. Dong, P. Shum, N. Q. Ngo, and C. C. Chan, "Multiwavelength Raman fiber laser with a continuously-tunable spacing," *Opt. Exp.*, vol. 14, no. 8, pp. 3288–3293, Apr. 2006.

[9] M. A. Ummy, N. Madamopoulos, A. Joyo, M. Kouar, and R. Dorsinville, "Tunable multi-wavelength SOA based linear cavity dual-output port fiber laser using Lyot–Sagnac loop mirror," *Opt. Exp.*, vol. 19, no. 4, pp. 3202–3211, Feb. 2011.

[10] T. Torounidis and P. Andrekson, "Broadband single-pumped fiber-optic parametric amplifiers," *IEEE Photon. Technol. Lett.*, vol. 19, no. 9, pp. 650–652, May 2007.

[11] D. Chen and B. Sun, "Multi-wavelength fiber optical parametric oscillator with ultra-narrow wavelength spacing," *Opt. Exp.*, vol. 18, no. 17, pp. 18 425–18 430, Aug. 2010.

[12] B. Sun *et al.*, "Wavelength-spacing-tunable double-pumped multiwavelength optical parametric oscillator based on a Mach–Zehnder interferometer," *J. Lightw. Technol.*, vol. 30, no. 12, pp. 1937–1942, Jun. 2012.

[13] B. Sun *et al.*, "Double-pumped multiwavelength fiber optical parametric oscillator based on a Sagnac loop filter," *Opt. Lett.*, vol. 37, no. 1, pp. 106–108, Jan. 2012.

[14] J. Li and L. R. Chen, "Tunable and reconfigurable multiwavelength fiber optical parametric oscillator with 25 GHz spacing," *Opt. Lett.*, vol. 35, no. 11, pp. 1872–1874, Jun. 2010.

[15] Z. Luo *et al.*, "Multiwavelength fiber optical parametric oscillator," *IEEE Photon. Technol. Lett.*, vol. 21, no. 21, pp. 1609–1611, Nov. 2009.

[16] R. H. Stolen and J. E. Bjorkholm, "Parametric amplification and frequency conversion in optical fibers," *IEEE J. Quantum Electron.*, vol. QE-18, no. 7, pp. 1062–1072, Jul. 1982.

[17] N. Bloembergen and Y. Shen, "Coupling between vibrations and light waves in Raman laser media," *Phys. Rev. Lett.*, vol. 12, no. 18, pp. 504–507, May 1964.

[18] A. S. Y. Hsieh *et al.*, "Combined effect of Raman and parametric gain on single-pump parametric amplifiers," *Opt. Exp.*, vol. 15, no. 13, pp. 8104–8114, Jun. 2007.

[19] F. Vanholsbeeck, P. Emplit, and S. Coen, "Complete experimental characterization of the influence of parametric four-wave mixing on stimulated Raman gain," *Opt. Lett.*, vol. 28, no. 20, pp. 1960–1962, Oct. 2003.

[20] M.-C. Ho, K. Uesaka, M. Marhic, Y. Akasaka, and L. G. Kazovsky, "200-nm-bandwidth fiber optical amplifier combining parametric and Raman gain," *J. Lightw. Technol.*, vol. 19, no. 7, pp. 977–981, Jul. 2001.

[21] G. P. Agrawal, *Nonlinear Fiber Optics*. San Diego, CA, USA: Academic, 2013.

[22] J. Hansryd, P. A. Andrekson, M. Westlund, J. Li, and P. Hedekvist, "Fiber-based optical parametric amplifiers and their applications," *IEEE J. Sel. Topics Quantum Electron.*, vol. 8, no. 3, pp. 506–520, May/Jun. 2002.

[23] A. R. Chraplyvy, "Limitations on lightwave communications imposed by optical-fiber nonlinearities," *J. Lightw. Technol.*, vol. 8, no. 10, pp. 1548–1557, Oct. 1990.